EFFECT OF ELECTRODE CONFIGURATION AND ELECTRONIC CONDUCTIVITY ON CURRENT DENSITY DISTRIBUTION MEASUREMENTS IN PEM FUEL CELLS

by

Dilip Natarajan and Trung Van Nguyen*

Department of Chemical and Petroleum Engineering

University of Kansas

Lawrence, KS 66045

Submitted as
A Research Paper

To

Dr. C. K. Dyer
The Journal of Power Sources
16 Seven Oaks Circle
Madison, New Jersey 07940-1314
USA

1st submission: February 11, 2004
Revised: March 16, 2004

Key words: PEM fuel cells, conventional gas distributor, current density distribution, segmented electrode, mathematical modeling

* Author to whom correspondence should be addressed

ABSTRACT

Current density and potential distribution measurements were conducted using a segmented current collector and flow field setup on membrane electrode assemblies prepared with segmented and un-segmented electrodes made from two different types of commercially available gas diffusion layers. Both galvanostatic and potentiostatic discharge modes were employed. Irrespective of the type of gas diffusion layer, when a common electrode was employed, significant performance variations were encountered between current collector segments in the constant–voltage mode, while the segment to segment variations were minimal in the constant current mode. Both types of discharge modes showed negligible variations between segments in the case of segmented electrode. A simple mathematical model was developed to assist in the interpretation of the experimental results. The differences in contact resistances between the current collectors and the gas diffusion layer, especially on the cathode side have been identified as the primary reason for the experimentally observed behavior. Based on the results presented here, segmenting the electrode along with the current collector is recommended for current distribution studies. When using a common electrode, only the galvanostatic mode is preferred to minimize contact artifacts.

INTRODUCTION

Fuel cells are fast becoming viable alternative energy conversion devices of the 21st century. Their high efficiency, simplicity in design and operation and pollution free characteristics make them an attractive option for terrestrial applications. Of the various types of fuel cells available, Proton Exchange Membrane (PEMFC) fuel cells are considered to be most suitable for transportation and portable applications due to attractive features like low operation temperature, high energy density and efficiency. However, their performance needs to be further optimized [1] to be cost competitive with current energy conversion devices like the internal combustion engine or batteries. Significant strides have been made towards addressing this goal of performance improvement and cost optimization through development of better membranes, improved catalyst layer fabrication techniques leading to better catalyst utilization [1] and better flow field designs that enhance reactant and product transport within the fuel cell [1,2].

Performance improvement in a typical PEM fuel cell directly translates to achieving higher average current per unit area (otherwise known as current density) at any given operating cell voltage or vice versa. On the other hand, uniformity of current density distribution across the entire active area is crucial for performance optimization. The local current density distribution within a PEM fuel cell is a function of various factors like local membrane hydration state, reactant and product concentration, temperature, etc. Over the past decade, experimental complications associated with PEM fuel cells due to their inherent small geometries and extreme aspect ratios, prompted researchers to develop representative first principles based mathematical models [3-18],

to gain qualitative information on membrane hydration, temperature and species concentration distribution. Pioneering work in fuel cell modeling were usually one dimensional, representing the direction normal to the reactive catalyst surface, and accounted only for gaseous phase to avoid the complexities involved in multi-dimensional modeling of multi-phase flow in porous media [3-6]. Though these models provide excellent qualitative information, to achieve representation of 'real life' situations, researchers have been looking into multi dimensional, multi phase models [7-18] to get a more accurate picture of the various transport and kinetic phenomena in PEM fuel cells employing different flow distribution strategies. While these models provide excellent qualitative information, experimental data on the local current density distribution in operating PEM fuel cells is essential to validate and verify the model predictions and to accurately estimate the various kinetic and transport parameters to develop these models into practical design tools.

BACKGROUND

In this section available literature on attempts to obtain such local current density distribution data is reviewed briefly. Cleghorn et. al. [19] conducted some pioneering current density distribution measurements on typical lab scale PEM fuel cell setups. The authors used Printed Circuit Board (PCB) technology to create a segmented current collector and flow field that was used on the anode with segmented gas diffusion layer and catalyst layer, while the cathode employed a regular un-segmented electrode, (i.e. diffusion and catalyst layer) current collector and flow field. The effects of anode and cathode stream humidity and stoichiometric flow rate of air on the steady-state current

density distribution were studied. The authors employed a combination of two load units and a specially designed patch board that acted as a multiplexer to control the voltage at the various segments. Stumper et. al. [20] analyzed three methods for current density distribution mapping namely the partial Membrane Electrode Assembly (MEA) approach, the subcell technique and the current mapping technique. The first approach involves the use of several different MEAs with a catalyzed active area of varying fractions of the total flow field area. In the sub cell approach the authors used a number of 'subcells' at various locations along the gas flow channel that were electrically insulated from the main active MEA and controlled by a separate load. In the third approach, a network of passive graphite resistors were placed between the flow field plate and the current collecting bus plate, while the potential drop across these resistors were monitored to establish the current flowing through them. Wieser et. al. [21] proposed the use of an array of Hall sensors with a segmented current collector and flow field for local current density measurements. The authors used un-segmented electrodes in their study.

While these techniques are no doubt quite innovative, they are not without disadvantages. The partial MEA approach does not provide sufficient spatial resolution and significant errors can arise due to inherent variations in electrical, transport and kinetic properties between different MEAs. The 'subcell' approach is plagued by the difficulty in properly isolating the 'subcells' from the main electrode and achieving perfect alignment of the anode and cathode sides. The use of Hall sensors can significantly complicate the experimental setup making experimentation expensive and tedious. Moreover interference from neighboring segments is also possible with the use of Hall sensors. A major cause of concern with the current mapping technique using

passive resistors is the lateral in-plane currents through the flow field plate that could lead to very low spatial resolution due to current spreading. The issue of significant lateral currents can be further complicated by differences in the contact resistance between the various resistors and the flow field plate. When using a single potentiostat, if the voltage sensing and control point is after the resistors the potential at the electrode will not be uniform because of the differences in the current flowing through the resistors. Though Cleghorn et. al.'s [19] approach avoids these complications, the use of a couple of load units with a multiplexer, (i.e., voltage control is quickly switched from one electrode to another by the multiplexer) only allows analysis of steady state behavior. Switching between electrodes gives rise to temporal double layer charging and discharging currents and could induce undesired transient artifacts. Barring the partial MEA approach, the problem associated with the use of a single potentiostat is common to all the other methods mentioned above.

Natarajan et. al. [22] presented some qualitative results on hydrogen starvation effects using segmented current collector and segmented electrode (diffusion and catalyst layers) setup on the anode side while using a single common electrode and current collector on the cathode side. The authors employed six segments along a single straight channel (corresponding to the conventional or serpentine flow field design) that were individually controlled by a multi-channel potentiostat/galvanostat to avoid the possible pit falls associated with the use of a single load and a multiplexer. Further details regarding the experimental setup are discussed in detail in the following sections. Brett et. al. [23] adopted the PCB technique introduced by Cleghorn et. al. [19] to a single straight channel cathode where each of the current collector ribs (10 in all) on the PCB

board was controlled by an individual load. They used a typical multi-channel anode with hydrogen flowing perpendicular (cross-flow) to the air stream. The electrodes on both sides of the MEA were not segmented. The authors have reported both steady state and transient results in their publication.

Recently Mench et. al. [24, 25] published some interesting steady-state and transient current density distribution data in Direct Methanol Fuel Cells [24] and PEM fuel cells [25]. They used specially built segmented flow fields with serpentine flow channels for both the anode and cathode sides, where the individual segments were separately controlled by a multi-channel potentiostat/galvanostat. The segmented flow fields were fabricated by embedding gold plated stainless steel ribs in a polycarbonate block. The authors employed commercially available MEAs where the electrodes were not segmented. Noponen et. al. [26] and Hottinen et. al. [27] adopted a similar approach to study steady-state and transient current density distributions in free-breathing PEM fuel cells.

Modifications like the use of segmented current collectors and individual control of segments using multiple potentiostats to the innovative techniques proposed by Stumper et. al. [20] and Cleghorn et. al. [19] eliminate problems like in-plane current spreading within the flow field plate or undesired transients caused by the multiplexer. However, apart from these advances one other major question to be addressed in current density distribution studies is whether the Gas Diffusion Layer (GDL) and the catalyst layer (i.e. the electrode) need to be segmented along with the current collector.

Current density distribution studies are aimed at obtaining information on the local reaction rate distribution within the catalyst layer which is a strong function of the

local electronic and ionic potentials, reactant and product concentration and membrane hydration state. Performance improvement and optimization of fuel cells directly relates to improving the electrochemical reaction rate within the catalyst layer. Hence an accurate picture of the local current density distribution as it emanates from the catalyst layer is of paramount interest to researchers from a fundamental point of view. In the case of a common GDL the question of whether one sees the same current distribution, as in the catalyst layer, at the current collectors depends on 1) The ratio of the normal distance from the current collector to the catalyst layer and electrode width along the channel, 2) The ratio of in-plane and through-plane area, 3) The ratio of in-plane and through-plane conductivities of the GDL material and finally, 4) The relative contact resistances between the GDL and the current collectors. The above mentioned parameters determine the extent of current spreading within the GDL. Mench et. al. [24, 25] implemented elaborate experimental techniques like the use of pressure indicating film to minimize contact resistance and assumed minimal current spreading or 'crosstalk' in their experiments with common GDLs. Another concern with the use of a common GDL is determining the active area associated with each current collector. Noponen et. al. [26] tried to address this by developing a simple model to estimate the errors arising from assigning equal areas to all the current collectors.

Experimental verification and quantification of the existence and extent of current dispersion within a common GDL in contact with multiple isolated current collectors are essential and is the focus of this work. This paper also emphasizes the need for segmenting the electrode in order to minimize the effect of variations in contact resistances between the electrode and the current collectors. A simple mathematical

model is also presented here to assist in the interpretation of the experimental results. The need for segmenting the electrode to correctly measure the true current density distribution within the catalyst layer is also emphasized. Finally, the significance of these results in terms of realistic PEM fuel cell model development is also discussed.

EXPERIMENTAL

Segmented Current Collector and Flow Field

Figure 1 is a schematic of the top and side view of the current collector and flow field block used in this work. Using a Computer Numerically Controlled (CNC) milling machine six rectangular grooves with precise dimensions of 50 mm (length) by 10 mm (width) by 4.85 mm (depth) were machined into a 140 mm by 70 mm block of acrylic. Bolt holes and pipe threaded gas holes were also machined into the block. Strips of the above mentioned dimensions were also machined out of a 5 mm thick POCO graphite plate using a CNC milling machine. The graphite plates were then gently pressed into these slots using a precision vice and quick setting 'super glue' was wicked into the gaps between the grooves and graphite. The protruding graphite surfaces were then machined flat using a sharp carbide 'fly cutter'. After polishing the surface on a fine sand-paper, a single gas channel was machined connecting the inlet and exit hole as shown in the figure. The acrylic block was an inch thick for the anode while the cathode graphite strips were placed in a ¼ ″ thick plastic block. A blank 1″ thick acrylic block and an aluminum heating block were also machined to contain pipe threaded gas holes and bolt slots. During cell assembly the aluminum heating block was placed on the cathode side with O-rings on the gas holes between the blank plate and the thinner acrylic base plate to

achieve better heat transfer. The major planar faces of all the above mentioned parts of the fuel cell assembly were machine finished and polished and were found to be even within 12.5 μm using a high precision dial indicator.

MEA Fabrication

Electrodes fabricated by catalyst coating on two different types of gas diffusion layers, namely SIGRACET® GDL 30 BC from SGL-CARBON, Inc. and Toray® carbon paper TGPH-120 from ETEK, Inc. were obtained from TVN systems Inc. The carbon papers were 330 μm and 350 μm thick respectively. The SIGRACET® diffusion layer had a Teflon® content of 5% by wt. while the Toray contained no added Teflon®. The catalyst loading on both types of GDL were about 0.35 gm Pt / cm^2. A schematic of the MEAs with segmented or un-segmented electrodes on both sides are provided in Figure 2. Electrode pieces (7 mm by 10 mm) were cut from the procured stock along with gaskets with slots for the active electrode and holes for bolts, using precise paper masks with dimensions marked on it using AUTOCAD. Using the gaskets as a frame to accurately arrange the electrodes, the electrodes were hot pressed to Nafion® 112 membranes at 135°C and 65 psi (based on total area including gaskets). A combination of Teflon® and silicone gaskets were used on both sides of the MEA. Though the fuel cell assembly was capable of handling six segments, MEAs were prepared to correspond to four current collector segments for the sake of clarity of experimental data. Moreover, it should be noted that the common MEA had a slightly greater active area (c.a. 15%) than the segmented MEA due to the region between the current collectors. It should be noted that in the segmented MEA, the electrodes on anode and cathode were segmented, while a common electrode was used on both sides in case of the common MEA.

Test Procedure

The machined parts of the fuel cell and the fabricated MEAs were carefully assembled to ensure proper alignment between the current collector and electrode edges. The cell was assembled in a press at the same pressure as the hot pressing step of 65 psi based on the entire cell area to avoid any distortion to the MEA due to excess compression. The cell was tested for gas leak and cross-over before actual testing. Hydrogen was provided to the anode (thick plate) through a bottle of de-ionized water held at 60 or 70°C while oxygen was supplied to the cathode sparged at room temperature. Hydrogen and oxygen flow rates employed in all the experiments were about 51.5 cm^3/min and 25.8 cm^3/min respectively. These numbers translates to 2 A/cm^2 for common MEA with an active area of 3.22 cm^2, while for the segmented MEA with an active area of 2.8 cm^2 they correspond to 2.3 A/cm^2. The four current collector segments that were in contact with the electrode were each controlled independently using a multi-channel potentiostat/ galvanostat from Arbin Systems through current and voltage leads connected directly to the graphite segments protruding on one side (see Figure 1). The MEAs were subjected to multiple cycles alternating between constant current and voltage staircases at 30°C. The staircase limits for the potentiostatic staircases were chosen to be open circuit voltage and 0.7 V while the galvanostatic staircases were cycled between open circuit and 100 mA per segment for the SIGRACET® diffusion layer and 50 mA per segment for the Toray GDL. These values for the cycle limits were so chosen to limit mass transfer effects caused by liquid water accumulation on the current density distribution. During these cycles the segments were held at each current or voltage for 3 minutes. Finally, once the MEAs were sufficiently massaged (evaluated based on

reproducibility between cycles) the data from the last galvanostatic and potentiostatic cycles were chosen for analysis.

RESULTS AND DISCUSSION

Figure 3 provides the experimental data in the form of polarization curves based on the current and voltage responses from the four segmented current collectors, using a MEA with segmented electrodes fabricated from a SIGRACET® gas diffusion layer. The solid lines represent data obtained from galvanostatic discharge, while the dashed line indicates potentiostatic discharge. Similar results for a MEA with a common (un-segmented) electrode using the same experimental setup and operating conditions are provided in Figure 4. The current densities for the common MEA were calculated assuming that the area above the plastic separator is evenly divided between adjacent current collectors. Figure 5 provides the total current from the entire cell (sum of the currents from each collector segment) verses the average voltage at the current collectors. Experimental data obtained from the MEAs prepared from Toray® diffusion layers are provided in the latter sections.

Figure 3 shows that in the case of the segmented MEA, for any given segment the polarization curves obtained by both types of discharges are very close to each other and that the segment to segment performances are also uniform (a spread within 5 – 7 mA at any given operating voltage or vice versa). On the other hand, Figure 4 indicates that in a common (un-segmented) MEA, while the polarization curves from the four collectors are quite close to each other in the constant current discharge mode (within 5mV at 100 mA), there exists a significant spread in performance from segment to segment under constant

voltage mode (40 mA at 0.725 V). The difference between the segments under potentiostatic mode seems to increase with decreasing cell voltage. It should be noted here that the gas flow rates in these experiments were chosen such that there were negligible concentration variations along the channel. Moreover, on comparing Figures 3 and 4 it is evident that the polarization curves obtained in the galvanostatic or constant current discharge mode for two types of MEAs match quite satisfactorily, showing that the electrodes obtained from TVN systems have consistent catalytic properties. The overall performances are identical in Figure 5 for both the segmented and un-segmented MEAs, irrespective of the discharge mode. Based on the results seen in Figure 5 it can be inferred that there are no significant differences in terms of overall activation, ohmic and mass transport properties between the two types of MEA and that the discharge mode does not affect the overall cell performance. Slightly greater area between the current collectors in the common MEA seems to have a negligible effect probably due to lack of electronic contact.

Having established that the overall properties of the two MEAs are quite similar, the question is whether it is significant local variations in the ohmic, transport or kinetic properties along the length of the channel that causes non-uniformity in the case of common MEA under potentiostatic discharge. Ideally, if all relevant properties are invariant along the channel length, the individual segment performances should be identical under the chosen operating conditions (that ensures no change in reactant or product concentrations along the channel) irrespective of the electrode configuration or discharge mode. If this was possible, segmenting the electrode would be unnecessary. However, the individual segment polarization curves shown here suggest that there are

indeed variations in segment performances in the case of the common MEA which are mitigated by segmenting the electrodes. For the common MEA, the fact that discharge mode has an effect on the variations in segment performances suggest some kind of segment to segment interactions.

In a segmented MEA, by isolating the electrodes physically, all interactions between segments are eliminated barring the common membrane and a shared gas channel. Hence one would expect to see the segments act as independent single cells with no interference from the neighboring segments under certain operating conditions that do not induce any variations in reactant and product concentrations. However, variability could exist between segments due to inherent differences in local membrane properties or variations in contact resistances. Under subtle operating conditions used here, such as using pure humidified hydrogen and oxygen and low reaction demand that do not induce significant concentration variations along the channel, the results from the segmented MEA suggest no interaction between segments as expected and it is also encouraging to note that segmented MEAs can be fabricated with comparable segment properties.

In a common electrode there can be interferences between segments due to differences in local properties of the electrode. Liquid water dynamics between the regions under two adjacent current collectors may play a role in these segment to segment interactions. However, the extreme aspect ratio between the direction along the channel and that normal to the reactive interface and the drastic differences in the available cross-sectional area for flow in these two directions are expected to significantly limit this liquid transport interaction. Also, liquid water flooding effects also affect the overall performance of the MEA which was not the case here. Moreover, the fact that the

common MEA shows very similar segment performances under galvanostatic mode and not under potentiostatic mode (while segmented MEA results were similar for both discharge modes) lead us to believe that the interactions could be electronic and not kinetic in nature. Electronic interactions arise mainly due to differences in contact resistances between the various current collector segments and the GDL (assuming uniformity in GDL/electrode electronic properties). However, the similarity between the two types of discharges and lack of significant segment to segment variations in the segmented MEA suggests reasonable uniformity in contact, which is counter-intuitive to our previous hypothesis on electronic interactions. In-depth information on the potential and current vector distribution within the diffusion layer for the two types of MEAs under different discharge modes is essential to verify the validity of our hypothesis about electronic interactions in a common MEA and to obtain a clear understanding of the phenomena involved. Hence a simple model was developed to assist in the interpretation of the experimental results and is presented in the following sections.

Modeling

A two-dimensional mathematical model was developed to map the solid phase potential (ϕ) distribution. The model domain is presented in Figure 6 along with the various boundaries and dimensions. The domain included half of two adjacent current collectors in contact with a common diffusion layer, with a plastic shoulder separating the current collectors. The model accounts for the dimension in the channel direction along which the current collector segments are placed (X direction) and the dimension normal

to the reactive interface (Y direction). The governing equations and boundary conditions are provided below.

Governing equations

Within the gas diffusion layer: $$-\left(\sigma_{X,GDL}\frac{\partial^2\Phi}{\partial X^2}+\sigma_{Y,GDL}\frac{\partial^2\Phi}{\partial Y^2}\right)=0 \qquad [1]$$

Within current collectors A & B: $$-\sigma_{CC}\left(\frac{\partial^2\Phi}{\partial X^2}+\frac{\partial^2\Phi}{\partial Y^2}\right)=0 \qquad [2]$$

Within the plastic separator: $$\Phi = 0.0 \qquad [3]$$

Boundary conditions

At boundaries 2, 4, 3-S, 5-A & 5-B: $\vec{n}\cdot\nabla\Phi = 0$ where $\vec{n}$ is the unit vector in the normal direction

At the boundary 3-A: $$-\left(\sigma_{Y,GDL}\frac{\partial\Phi}{\partial Y}\right)=-\left(\frac{\left|\Delta\Phi_A\right|}{R_{CON,A}}\right)=-\left(\sigma_{CC}\frac{\partial\Phi}{\partial Y}\right) \qquad [4]$$

At the boundary 3-B: $$-\left(\sigma_{Y,GDL}\frac{\partial\Phi}{\partial Y}\right)=-\left(\frac{\left|\Delta\Phi_B\right|}{R_{CON,B}}\right)=-\left(\sigma_{CC}\frac{\partial\Phi}{\partial Y}\right) \qquad [5]$$

At the boundary 6-A & 6-B: $$-\left(\sigma_{CC}\frac{\partial\Phi}{\partial Y}\right)=I_{APP} \quad \text{(or)} \qquad \Phi = V_{APP} \qquad [6]$$

At the reactive interface 1: $$-\left(\sigma_{Y,GDL}\frac{\partial\Phi}{\partial Y}\right)=-i_O\left(10^{\left[\frac{\Phi-E^O}{\eta_C}\right]}-10^{\left[\frac{-\left(\Phi-E^O\right)}{\eta_C}\right]}\right) \qquad [7]$$

Here $\sigma_{X,GDL}$ and $\sigma_{Y,GDL}$ stand for the in-plane, through-plane conductivities of the gas diffusion layer, σ_{CC} represents the bulk conductivity of the current collector, $R_{CON,A}$ and $R_{CON,B}$ are the areal contact resistances between current collectors A and B and the GDL,

and $\Delta\Phi_A$ and $\Delta\Phi_B$ are the potential drops at the corresponding interfaces due to contact resistance. The reader is referred to the 'list of symbols' section for explanation on other variables. The partial differential equations were discretized using finite difference method and the resulting algebraic equations were solved using a banded matrix solver [28].

As can be seen from the boundary conditions, the model was setup to accommodate both galvanostatic and potentiostatic simulations. The boundary condition at interface 1 was set to represent the slow oxygen reduction reaction in most cases. The model was used to simulate galvanostatic and potentiostatic discharges employing segmented and un-segmented SIGRACET® and Toray® gas diffusion layers. Toray® GDL with different electronic properties was included in these simulations to validate the qualitative predictions of this model. The relevant model parameters are provided in Table 1. The exchange current density was adjusted to provide the current densities in the range of the experimental values. The exchange current density values used in these simulations are comparable to values reported in literature for ORR kinetics at Platinum/Nafion® interface at 30°C [29, 30]. The Tafel slope for ORR kinetics chosen for these simulations was also close to reported literature values [29, 30]. The through-plane conductivity of SIGRACET® GDL was obtained from the manufacturer. The in-plane conductivity was estimated by a four probe conductivity measurement technique and the order of magnitude of the measured value was also verified by the manufacturer. Both in-plane and through-plane conductivity for Toray® gas diffusion layers were obtained from the manufacturer and verified using a four probe milliohmmeter. The bulk conductivity of POCO graphite was obtained from the literature [31].

The contact resistances between the segmented current collectors and the diffusion layers were estimated experimentally. The segmented plates were assembled with just a SIGRACET® or Toray® GDL of known dimensions under a compression pressure of 65 psi. Moreover, a silicone gasket was used as a frame to position the carbon paper accurately on the segmented current collectors. Though these measurements may not reflect the true contact resistances when an actual MEA is used, they should still provide a reasonable range. This type of assembly includes the inherent through-plane resistance of the GDL and contact resistances at both faces of the GDL. Measurements were conducted on multiple specimens for both types of GDL for all the current collectors at varying current densities and the results are tabulated in Table 2. The values provided in Table 2 were based on the total geometric area of the GDL and not just the shoulder area of the current collectors. Hence the actual contact resistances encountered is probably slightly lower. The range of the measured contact resistance values for the two types of GDL were very similar as expected. To this author's knowledge, even the high end of the range of contact resistances in Table 2 is among the lowest reported in the literature. Mench et. al. [25] reported an average contact resistance of 0.0417 Ω-cm^2. Barbir et. al. [32] suggest contact resistances as high as 0.15 Ω-cm^2. Mepsted et. al. [31] conducted a comprehensive study on different materials used for bipolar plates and concluded that graphite plates offer the lowest contact resistance (or surface resistivity) of all the materials. Their measured graphite-graphite contact resistance was about 0.014 Ω-cm^2 (for the sake of comparison). Based on the values reported in Table 2 it is also seen that the lower end of the range of areal contact resistances is almost the same as that of the through – plane areal resistance of the SIGRACET® GDL.

Initially the areal contact resistances for both the current collectors simulated in the model were assigned the same value (0.0105 Ω-cm^2) as that of the through-plane areal resistance of the gas diffusion layer (SIGRACET®). The 'Y' direction thickness of the current collector was arbitrarily chosen to be 330 μm. The thickness of the bulk current collectors is not crucial as the potential drop in the current collectors were expected to be negligible. When the contact resistances were uniform, the simulation results for both discharge modes were symmetrical about the mid point on the plastic separator and the current or voltage responses at the two collectors were identical as expected (results are not provided here for the sake of brevity). The areal contact resistance at current collector B was then doubled to correspond to the highest measured areal contact resistance (0.021 Ω-cm^2).

The results of this simulation (both constant current and constant voltage mode) for a SIGRACET® GDL are provided in Figure 7. Qualitatively, the model predictions match quite well with the experimental results presented in Figure 4. The significant discrepancy in the ordinate (cell voltage) axis can be attributed to the fact that the simple model developed here does not account for the potential losses at the membrane and anode. Nevertheless the model simulations capture the differences encountered between the two types of discharge modes. It is evident that the differences in the polarization behavior between constant current and constant voltage mode observed in experiments is clearly due to differences in contact resistances between the current collector segments and the GDL. It should be noted that the kinetic parameters were held constant in these simulations. The case of segmented electrodes was also simulated by arbitrarily decreasing the in-plane conductivity of the GDL by two orders of magnitude. The results

are presented in Figure 8. Similar to the experimental data shown in Figure 3, when the electrodes are segmented, the polarization curves lie on top of each other irrespective of the discharge mode. One of the major concerns among the fuel cell research community regarding segmenting electrodes is achieving uniform comparable contact and performance from segment to segment [21-27]. The experimental and model results suggest that, small differences in contact resistances do not significantly manifest themselves when the electrode is segmented. On the other hand despite similarity in kinetic and transport properties the same difference in contact resistances significantly affects the results in the case of the common MEA, especially in the constant voltage mode.

To further understand this behavior, the potential and electronic flux vector distributions within the common GDL are mapped in Figures 9 & 10 for the two types of discharges. Figures 9a and 10a clearly show a symmetric potential and electronic flux distribution within the gas diffusion layer for the case of the galvanostatic simulation. The solid potential has a greater drop at the interface between the current collector B and the GDL due to the higher contact resistance. As expected, the potential drop within the current collectors is negligible. The potentiostatic simulations shown in Figures 9b and 10b show a drop in the potential within the GDL from the region above current collector B towards the region over current collector A indicating the existence of in-plane current flow within the GDL. The electronic flux vector plot confirms this phenomenon indicating flow of electrons from current collector A towards the regions over current collector B. Thus despite the significant geometric size differences associated with the in-plane and through-plane directions, there exists significant interactions between

segments. This is probably due to the inherent higher in-plane conductivity compared to through-plane values of typical GDL material (see Table 1) arising from carbon fiber orientation. Noponen et. al. [27] used the through-plane resistance of the GDL in all directions in their model and hence did not observe a similar phenomenon.

Ignoring bulk collector losses the total voltage drop between the reactive interface and the voltage sensing point in the current collector can be expressed as $\Delta V = \Delta V_{CON} + \Delta V_{GDL} + \Delta V_K$, where ΔV_{CON} is the potential loss associated with contact, ΔV_{GDL} is the loss across the diffusion layer and ΔV_K is the activation loss. During galvanostatic control, ΔV_{GDL} and ΔV_K are fixed by the current demand per segment. Hence the only difference between the segments would arise out of the differences in contact between current collectors and GDL, which are quite small. In the case of potentiostatic control, however, all the three losses mentioned above vary. The potential at the reactive interface depends on both the contact and GDL losses and due to the exponential nature of the kinetic term, differences in the solid potentials at the reactive interface can result in significant variations in the current distribution.

Fuel cell researchers usually assume uniformity in local current density distribution in the kinetic region. However, these results clearly indicate that in un-segmented electrodes, non-uniformity in contact resistances manifest themselves significantly (depending on the discharge mode), even in the low-current density activation region and such an assumption is not appropriate if uniform contact cannot be achieved. Though this study is limited to the low current density region, the effects of contact variations will persist over the entire operating range of potentials (or current density) and can be expected to grow in significance with increasing current densities.

However, transport pertaining to liquid water dynamics will eventually start to gain significance and this phenomenon might mask the electronic interactions between the segments. Hence, it essential to first study the effect of contact resistance variations at low current density region where liquid water influences are minimal. Once these contact issues are addressed, the interactions between segments at higher current densities can be easily discerned from liquid water effects, given the linear dependence of ohmic effects on current densities.

It should be noted that the experimental results were generated using either segmented or un-segmented electrodes on both the anode and cathode. Hence differences in contact resistances on the anode side were also evaluated using the model. Equation 7 that represents the boundary condition at the reactive interface was replaced by a simple linear expression shown in Equation 8 to capture the facile anode kinetics.

$$-\left(\sigma_{Y,GDL}\frac{\partial\Phi}{\partial Y}\right)=\frac{\left(\Phi-E^{O}\right)}{\eta_{A}} \qquad [8]$$

where η_A has a value [33] of 40 mV per A/cm^2 . All other parameters were kept the same as that of the cathode simulations. Once again the model simulations were symmetrical about the plastic separator midpoint and the segment performances were identical when the contact resistances were kept the same for the two current collectors. The simulation results for current collectors with different contact resistances are presented in Figures 11a and 11b for a common and segmented anode. These results are significantly different from the cathode. While the linear current–voltage response is expected, it can be seen that the two segments do not perform uniformly in both MEAs irrespective of the discharge mode. Like the cathode, during potentiostatic runs on the anode, all the potential losses associated with current flow are variables and are ultimately related to the

differential contact, leading to performance variations between segments. In the case of galvanostatic mode, once again the difference between segment performances is mainly controlled by the differences in contact. Unlike the cathode where the large kinetic losses masks these differences, in the anode the contact losses are comparable to the activation loss and manifest themselves even in the constant current mode of operation leading to some interaction between segments. One important point to note is that the differences in the simulated performance from segment to segment is quite negligible at the anode (c.a.1 mV) when compared to the cathode (10 -12 mV) at a given current density (c.a. 100 mA). Hence the cathode contributes mostly to the differences between segment performances seen in the experiments. These model results for the anode suggest that any difference in contact will show up irrespective of the whether the electrode is segmented or un-segmented. However, the differences caused by the differential contact at the anode have negligible contribution to the overall interaction between segments.

Experiments and model simulations were also conducted on Toray® gas diffusion layers to further verify the observations discussed in the previous sections. The Toray® GDL has a higher bulk density and lower porosity. Hence the conductivities in both the in – plane and through-plane directions are much higher (see Tables 1 and 2). Figures 12 and 13 provide the experimental data on segmented and un-segmented (common) MEAs prepared using Toray® carbon paper while the overall performances are compared in Figure 14. The trends represented in these figures are quite similar to results from SIGRACET® GDL. Here again, segmented MEAs provide polarization curves that are almost identical irrespective of the discharge mode. The common MEA shows significant differences in the individual collector performances under potentiostatic mode while the

galvanostatic curves are very close to each other. As before, Figure 14 does not indicate any significant difference between the two MEAs in terms of overall performance validating the need for a segmented electrode and current collector setup for local current density distribution studies. The individual segment and overall performances were in general lower than the SIGRACET® GDL. This was probably due to the lower porosity of the Toray® diffusion layer resulting in poorer gas and liquid water transport leading to lower oxygen concentration at the interface. Interestingly, in the constant voltage mode, the segments (3 and 4) that tends to deviate from the galvanostatic curves seems to be consistent between the two type of diffusion layers (SIGRACET® and Toray®).

The corresponding model results for common and segmented MEAs fabricated with Toray® GDL are presented in Figures 15 and 16. In these simulations, the effective exchange current density was reduced by half to allow for the model simulations to roughly match the current density range obtained in the experiments. Other than exchange current density and the relevant conductivity values, no other changes were made to the model parameters. The contact resistances were kept the same as before since experimentally measured values for the two types of GDL were in the same range. The model results in Figures 15 and 16 qualitatively match the experimental results for Toray® GDL. Once again the spread in the polarization curves for a common MEA on constant voltage mode caused by differential contact is consistent with experimental results.

The model and experimental results from the two types of diffusion layers clearly show that inter-segment interactions in common MEA can be avoided only if the differences in segmented current collector-MEA contact resistances are minimal. As

mentioned before, the contact resistances measured in this study are among the lowest reported values and achieving further uniformity at this scale can be very difficult. Moreover the same differences in contact that also existed in the case of a segmented MEA did not significantly affect the uniformity in the segment performances. It should also be noted that when using segmented electrodes, the distance between the segments (and hence the segmented current collectors) is not crucial as long as no concentration variations are introduced along the channel.

Finally, the question of whether the common membrane affects the current density distribution in terms of segment to segment interaction needs to be addressed. The ionic conductivity of even a well hydrated membrane is usually about two orders of magnitude smaller than the electronic conductivity of the electrode. Though the local membrane conductivity is a strong function of the hydration state of the membrane which can vary along the channel depending on the operating conditions like flow rates, humidity, temperature, etc., currently there is no evidence of any anisotropy in conductivity of the membrane used in this study, unlike the electrode. In other words, the overall conductivity of the membrane is expected to be the same in the normal direction and the direction along the channel. Also, typical aspect ratios related to the membranes (50μm by few mm for Nafion® 112) are also more extreme than that of the electrode. (175-350 μm by few mm). Based on these observations, minimal segment to segment interactions or 'crosstalk' is expected across the membrane when a MEA with segmented electrodes and common membrane is used for current density distribution studies. Qualitative evidence for this hypothesis was presented by Natarajan et. al. [34]. The

authors showed that the differences in segment performances were insignificant for segmented electrode MEAs with common and segmented membrane.

As mentioned earlier in the introduction section, sophisticated models have been developed to capture the two-phase transport and electro-kinetic phenomena in a PEM fuel cell. Reasonably accurate estimates of the various physical and chemical properties of the components of the PEM fuel cell are essential to transform these models into predictive tools, for which relevant experimental data are needed. Important kinetic parameters such as the intrinsic exchange current densities for platinum catalyzed H_2 oxidation and O_2 reduction reactions have been experimentally estimated and methods to extrapolate these results to porous catalyst layers such as in PEM fuel cells have been established [29, 30 & 35]. However, there is a lack of information on physical properties of the gas diffusion layers such as gas and liquid water permeability and their dependence on liquid water saturation, the functional dependence of capillary pressure on saturation etc. Fuel cell researchers have attempted to come up with estimates for these gas and liquid transport parameters by comparing experimental data to model predictions [14, 17 & 36]. Natarajan et. al. [14] for instance, studied the effect of model domain selection (2-D vs. 3-D) on permeability and capillary function estimates for the GDL in a PEM fuel cell. Their work, suggests a clear need for a robust three dimensional model along with experimental data on local current density distribution at various operating conditions to accurately estimate such GDL properties. Segmented fuel cell assemblies are needed to generate such local current density distribution data.

The information provided in this paper clearly demonstrates that the significant difference between the in-plane and through-plane conductivities of the GDL and

variations in contact resistances affects the local current density distribution, when only the current collector is segmented and the electrode is not. Experimental results from such a setup can only be compared to models where the electronic properties of the GDL and contact resistance variations are properly accounted for. Most of the models that is available in the literature deal with an un-segmented electrode and do not explicitly account for the electronic properties of the GDL and variations in contact resistance which affects the solid potential distribution and hence the local current density. A few models [9] do account for the electronic conduction in the solid phase, but only in terms of a heat source (Joule heating) that affects the temperature distribution. Such an approach can only be justified if it is assumed that the effect of variations in contact resistance is minimal. The results provided here clearly show that by segmenting the electrode this assumption of minimal contact effects is satisfied. Then the remaining questions are 1. Whether there exists significant liquid water movement within the gas diffusion layer in the direction along the channel which might affect the local current density distribution (i.e. along the direction suggested for electrode segmentation) and would segmenting the electrode unrealistically eliminate such a transport feature? and consequently 2. Can data from segmented electrode studies be compared to model predictions based on common electrodes? As mentioned before, owing to the extreme aspect ratio of the PEM fuel cell electrode and the related differences in area for flow, it is expected that liquid water transport within the GDL along the channel will be minimal and segmenting the electrodes would still capture the current density distribution that one can expect in an ideal (with minimal contact influences) un-segmented electrode. This hypothesis can be further justified by the fact that while transport properties within the

GDL are expected to be isotropic (as long as the structure, morphology and Teflon content distributions are uniform across the GDL), current GDL materials do exhibit significant anisotropy when it comes to electronic conductivity.

CONCLUSIONS

Current density distribution measurements under galvanostatic (constant-current) and potentiostatic (constant-voltage) modes were carried out on membrane electrode assemblies fabricated with segmented and un-segmented electrodes using a segmented current collector and flow field setup. Two commercially available gas diffusion layers, namely SIGRACET® GDL 30 BC from SGL-CARBON, Inc. and Toray® carbon paper TGPH-120 from ETEK, Inc., were studied.

For both types of GDL, when the electrode was not segmented, the individual segment performances showed significant variations when discharged at constant voltage and the variations were minimal under galvanostatic mode. The overall cell performances, however, were very similar between the two types of discharges.

In the case of both the SIGRACET® and Toray®, the polarization curves of the individual segments did not show significant differences irrespective of the discharge mode when the electrodes were segmented. Here again the overall performances of the MEA were identical between the constant-current and constant-voltage modes.

A simple two-dimensional mathematical model was developed to map the potential distribution in the electrode. The model simulations qualitatively matched the experimental results and also proved that variation in contact resistances between the

current collectors and GDL especially on the cathode side was the primary cause for phenomenon observed in the experiments.

Based on the experimental and model results, for current density distribution studies, segmenting the electrode along with the current collectors is recommended. Inherent small variations in contact resistances between the various current collectors and GDL do not significantly manifest themselves in the case of segmented electrode configuration, irrespective of discharge mode. On the contrary, when using a common electrode, the same inherent contact variations will significantly affect the current density distribution when the segments are discharged in the potentiostatic mode. It is preferable to employ the constant-current mode of discharge for common electrode configurations to minimize variations in the performance due to contact differences. However it should be recognized that applying constant current density at every current collector does not represent actual fuel cell operating condition where only the average current density over the entire fuel cell (single cell or stack) is specified.

Acknowledgements

This work was supported by the National Science Foundation under Grant No. CTS-9910923.

Notation

Φ - Potential (V)

$\sigma_{X,GDL}$ - Through-plane conductivity of gas diffusion layer (S/cm)

$\sigma_{Y,GDL}$ - In-plane conductivity of gas diffusion layer (S/cm)

σ_{CC} - Bulk conductivity of POCO graphite current collector (S/cm)

$R_{CON,A}$ - Areal contact resistance between current collector A and gas diffusion layer (Ω-cm^2)

$R_{CON,B}$ - Areal contact resistance between current collector B and GDL (Ω-cm^2)

I_{APP} - Applied current (A/cm^2)

V_{APP} - Applied voltage (V)

E^O - Equilibrium potential (V)

η_C - Cathode Tafel slope (V/decade)

η_A - Empirical anode kinetic slope (V per A/cm^2)

i_O - Apparent exchange current density (A/cm^2)

ΔV - Total voltage drop from the sensing point to the reactive interface (V)

ΔV_{CON} - Voltage drop due to contact resistance (V)

ΔV_{GDL} - Voltage drop across the gas diffusion layer (V)

ΔV_K - Voltage drop due to activation (V)

References

1. S. Gottesfeld, and T.A. Zawodzinski, "Polymer Electrolyte Fuel Cells", in *Advances in Electrochemical Science and Engineering,* **5**, R.C. Alkire, H. Gerischer, D.M. Kolb and C.W. Tobias, Eds., Wiley-VCH, New York, 195 (1997).
2. T. V. Nguyen, *J. Electrochem. Soc.*, **143**, L105 (1996).
3. T. E. Springer, M. S. Wilson and S. Gottesfeld, *J. Electrochem. Soc.*, **140**, 3513 (1993).
4. Renaut Mosdale and Supramaniam Srinivasan, *J. Electrochimica Acta,* **40,** 413 (1995).
5. D. M. Bernardi and M. W. Verbrugge, *J. Electrochem. Soc.*, **139**, 2477 (1992).
6. M. L. Perry, J. Newman and E.J. Cairns, *J. Electrochem. Soc.*, **145**, 5 (1998).
7. T. V. Nguyen and R. E. White, *J. Electrochem. Soc.*, **140**, 2178 (1993).
8. A. C. West and T.F. Fuller, *J. Applied Electrochemistry*, **26**, 57 (1996).
9. V. Gurau, H. Liu and S. Kakac, *AIChE Journal*, **44**, 2410 (1998).
10. D. Singh, D. M. Lu and N. Djilali, *Int. J. Eng. Sci.,* **37**, 431 (1999).
11. S. Dutta, S. Shimpalee and J. W. Van Zee, *J. Applied Electrochemistry*, **30**, 135 (2000).
12. S. Shimpalee and S. Dutta, *J. Numerical Heat Transfer,* Part A, **38,** 111 (2000).
13. D. Natarajan and T. V. Nguyen, *J. Electrochem. Soc.*, **148**, 1324 (2001).
14. D. Natarajan and T. V. Nguyen, *J. Power Sources*, **115**, 66 (2003).
15. J. S. Yi and T. V. Nguyen, *J. Electrochem. Soc.*, **146**, 38 (1999).

16. J. S. Yi and T. V. Nguyen, " A Two-Phase Flow Model to Investigate the Hydrodynamics of Gas and Liquid water in the Cathode of PEM Fuel Cells with Interdigitated Gas Distributors," Paper 107b, *AIChE Meeting*, Miami Beach, FL Nov.15-20, 1998.

17. W. He, J. S. Yi and T. V. Nguyen, *AIChE Journal*, **46**, 2053 (2000).

18. C. Y. Wang and P. Cheng, *Int. J. Heat Mass Transfer*, **39**, 3619 (1996).

19. S. J. C. Cleghorn, C. R. Derouin, M. S. Wilson and S. Gottesfeld, *J. Appl. Electrochem.,* **28**, 663 (1998).

20. J. Stumper, S. A. Campbell, D. P. Wilkinson, M. C. Johnson and M. Davis, *Electochim. Acta,* **43**, 3773 (1998).

21. Ch. Wieser, A. Helmbold and E. Gulzow, *J. Appl. Electrochem.,* **30**, 803 (2000).

22. D. Natarajan and T. V. Nguyen, "Experimental Investigation of Spatial-Temporal Current Distribution in a PEM Fuel Cell," AIChE 2000 Annual Meeting, Symposium on Fuel Cells, Systems and Processors II, paper No. 4, Los Angeles, CA, November 12-17, 2000.

23. D. J. L. Brett, S. Atkins, N. P. Brandon, V. Vesovic, N. Vasileiadis and A. R. Kucernak, *Electrochemistry Communications,* **3**, 628 (2001).

24. M. M. Mench and C. Y. Wang, *J. Electrochem. Soc.*, **150**, A79 (2003).

25. M. M. Mench and C. Y. Wang, *J. Electrochem. Soc.*, **150**, A1052 (2003).

26. M. Nopenen, T. Mennola, M. Mikkola, T. Hottinen and P. Lund, *J. Power Sources*, **106**, 304 (2002).

27. T. Hottinen, M. Nopenen, T. Mennola, O. Himanen, M. Mikkola and P. Lund, *J. Applied Electrochemistry*, **33**, 265 (2003).

28. T. V. Nguyen and R. E. White, *Comput. Chem. Eng.*, **11**, 543 (1987)

29. A. Parthasarathy, S. Srinivasan, A. J. Appleby, and C.R. Martin, *J. Electrochem. Soc*., **139**, 2530 (1992).

30. W. K. Paik, T. E. Springer and S. Srinivasan, *J. Electrochem. Soc.*, **136**, 644 (1989)

31. G. O. Mepsted and J. M. Moore, "Performance and Durability of Bipolar Plate Materials" in *Handbook of Fuel cells,* **3**, W. Vielstich, A. Lamm and H. A. Gasteiger, Eds., John Wiley & Sons, 286 (2003).

32. F. Barbir, J. Braun and J. Neutzler, *J.New Mat. Electrochem. Systems*, **2**, 197 (1999).

33. W. He, J. S. Yi and T. V. Nguyen, "Edge Effects on Reference Electrode Measurements in PEM fuel cells", *J. Electrochem. Soc.*, (in press).

34. D. Natarajan and T. V. Nguyen, *201st Meeting of The Electrochemical Society, Meeting Abstracts*, Vol. 2002-1, Abstract No. 129 (2002).

35. J. Newman, *Electrochemical Systems*, Prentice Hall, Inc., Englewood Cliffs, NJ (1973).

36. T. V. Nguyen and W. He, "Interdigitated Flow Field Design" in *Handbook of Fuel cells,* **3**, W. Vielstich, A. Lamm and H. A. Gasteiger, Eds., John Wiley & Sons, 286 (2003).

Table 1: Parameter values used in the model

	SIGRACET® GDL	**Toray® GDL**
In – plane conductivity for common MEA $\sigma_{X,GDL}$ (S/cm)	78.5	200.0
In – plane conductivity for segmented MEA $\sigma_{X,GDL}$ (S/cm)	0.785	2.0
Through – plane conductivity, $\sigma_{Y,GDL}$ (S/cm)	3.14	14.0
Areal contact resistance of collector A, $R_{CON,A}$ (Ω–cm^2)	0.0105	0.0105
Areal contact resistance of collector B, $R_{CON,B}$ (Ω–cm^2)	0.021	0.021
Bulk conductivity of collectors A&B, σ_{CC} (S/cm)	670	670
Exchange current density [29, 30] i_O at 30°C (A/cm^2)	5.0 X 10^{-9}	2.5 X 10^{-9}
Equilibrium potential E^O (V)	1.2	1.2
Cathode Tafel constant * [29, 30] η_C at 30°C (V/decade)	0.0693	0.0693

* Parthasarathy et al. [29] reported a η_C value of 60 mV/decade at 25°C, while a value of 65 mV/decade at 30°C was suggested by Paik et al. [30].

Table 2: Contact resistances measured for SIGRACET® and Toray® GDL

	Through – plane areal resistance of GDL (Ω–cm^2) *(obtained from manufacturer)*	**Range of measured total through -plane areal resistance (Ω–cm^2)** ***(includes GDL and contact resistances)***	**Range of calculated through -plane areal contact resistance (Ω–cm^2)**
SIGRACET®	0.0105	0.032 – 0.046	0.011 – 0.018
Toray®	0.0025	0.024 – 0.047	0.011 – 0.022

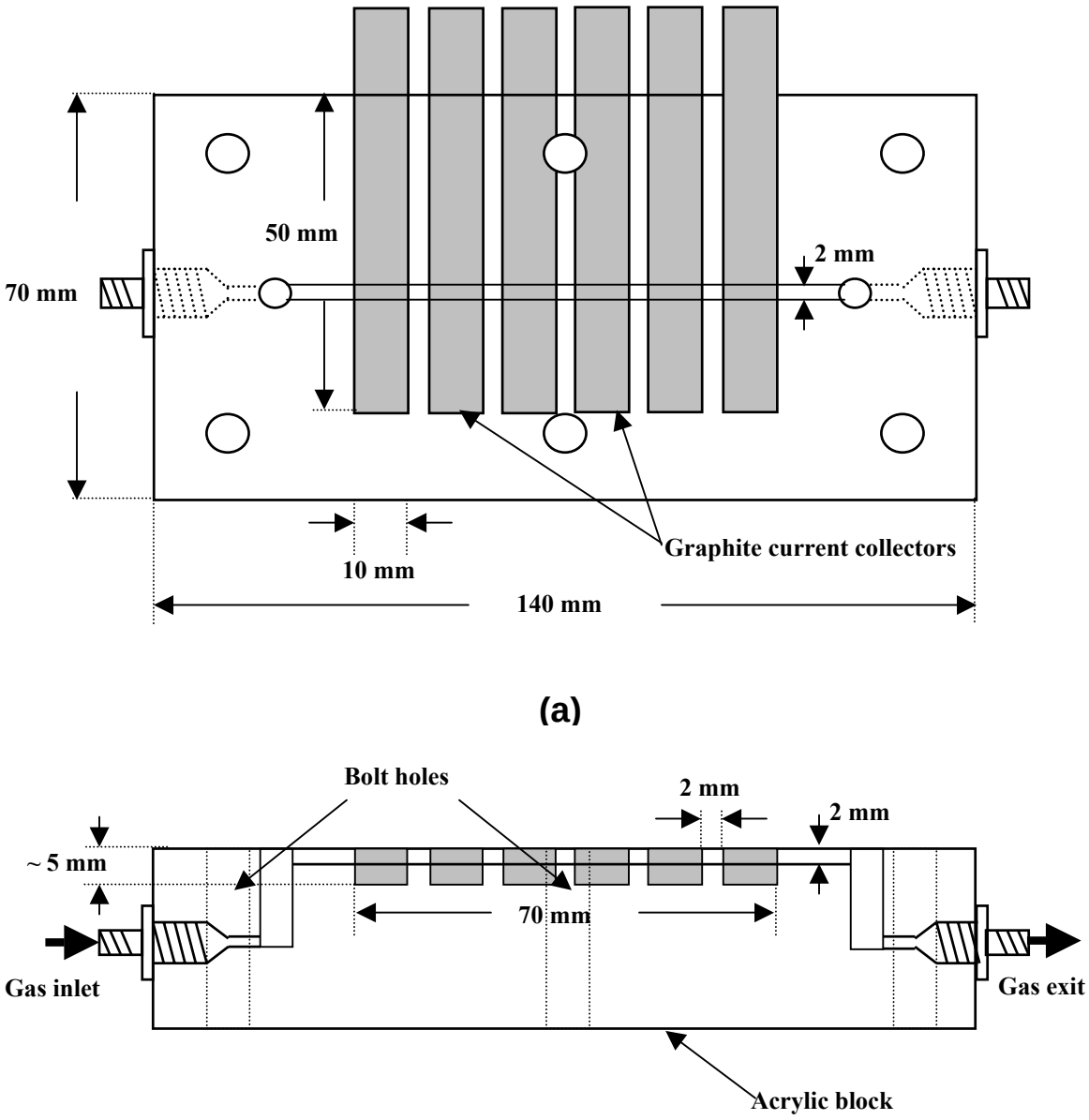

Figure 1: Schematic of the current collector and flow field block, (a) top view, (b) side view

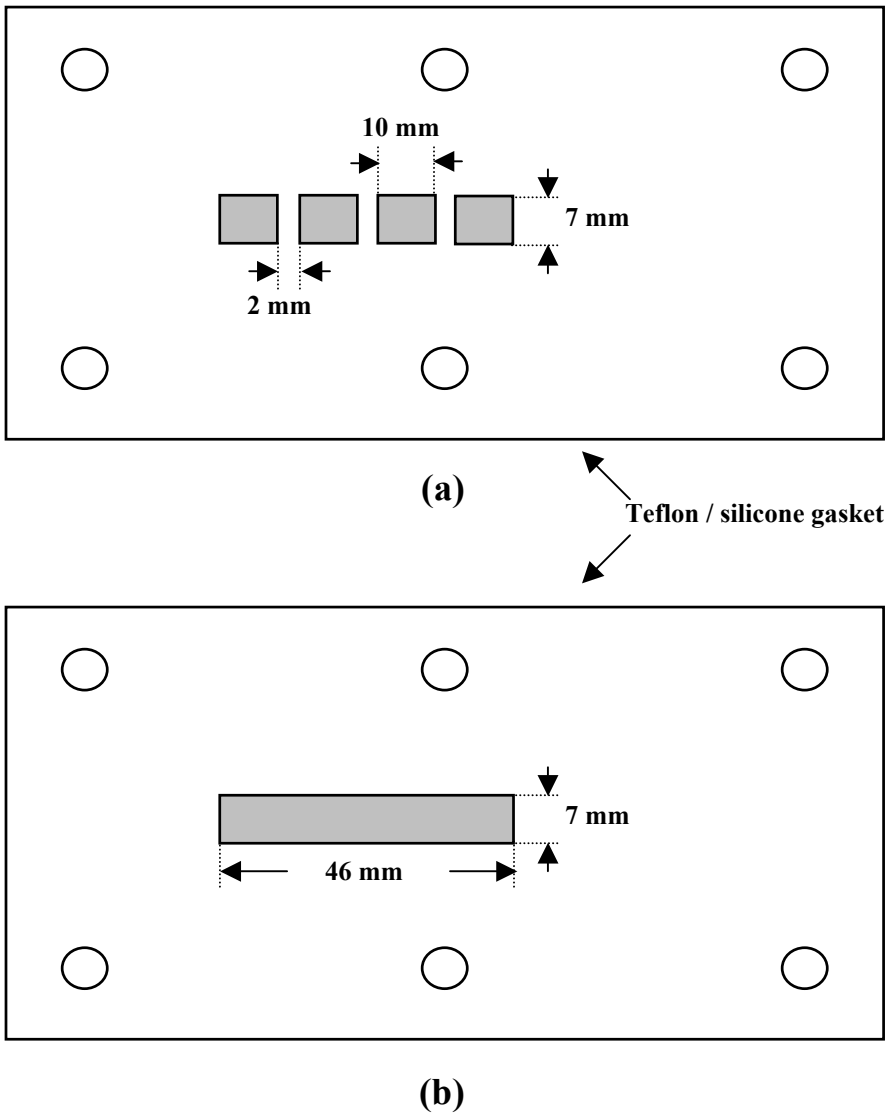

Figure 2: Schematic of the Membrane Electrode Assembly (MEA), (a) Segmented, (b) un-segmented

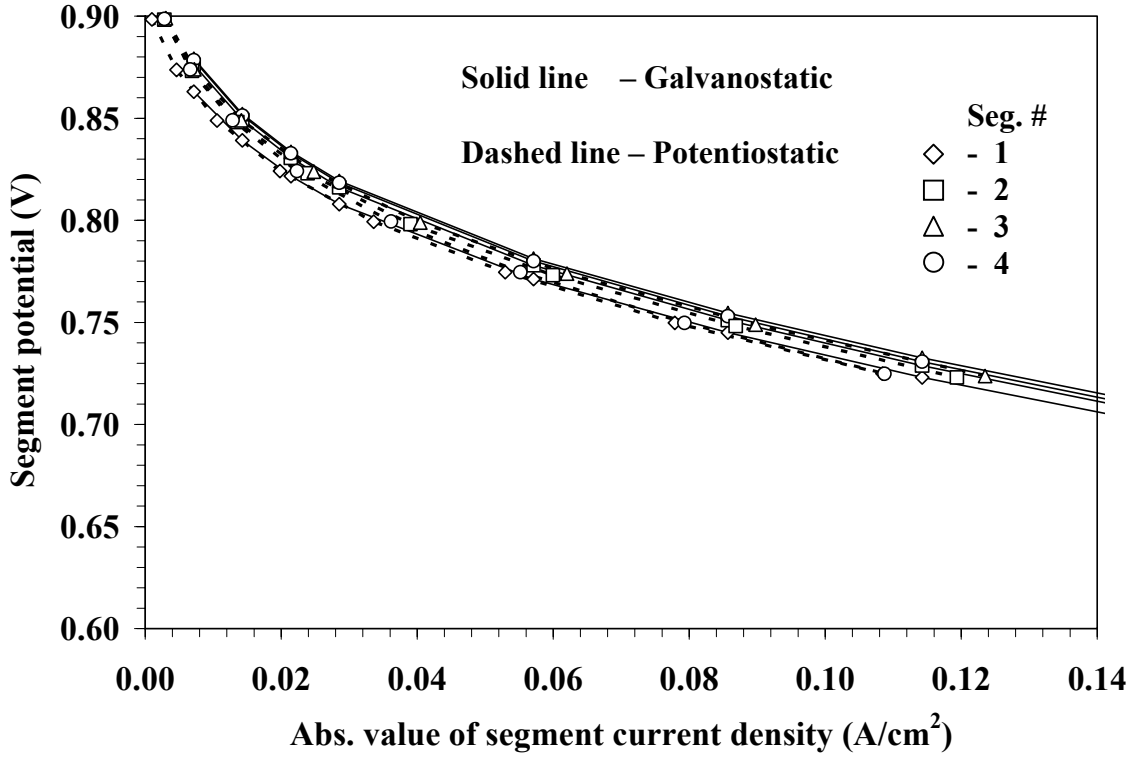

Figure 3. Galvanostatic and potentiostatic segment polarization curves using a segmented MEA with SIGRACET® GDL. H_2 flow rate = 2.3 A/cm^2, O_2 flow rate = 2.3 A/cm^2, H_2 humidifier temperature = 70°C, O_2 humidifier temperature = 25°C and Cell temperature = 30°C.

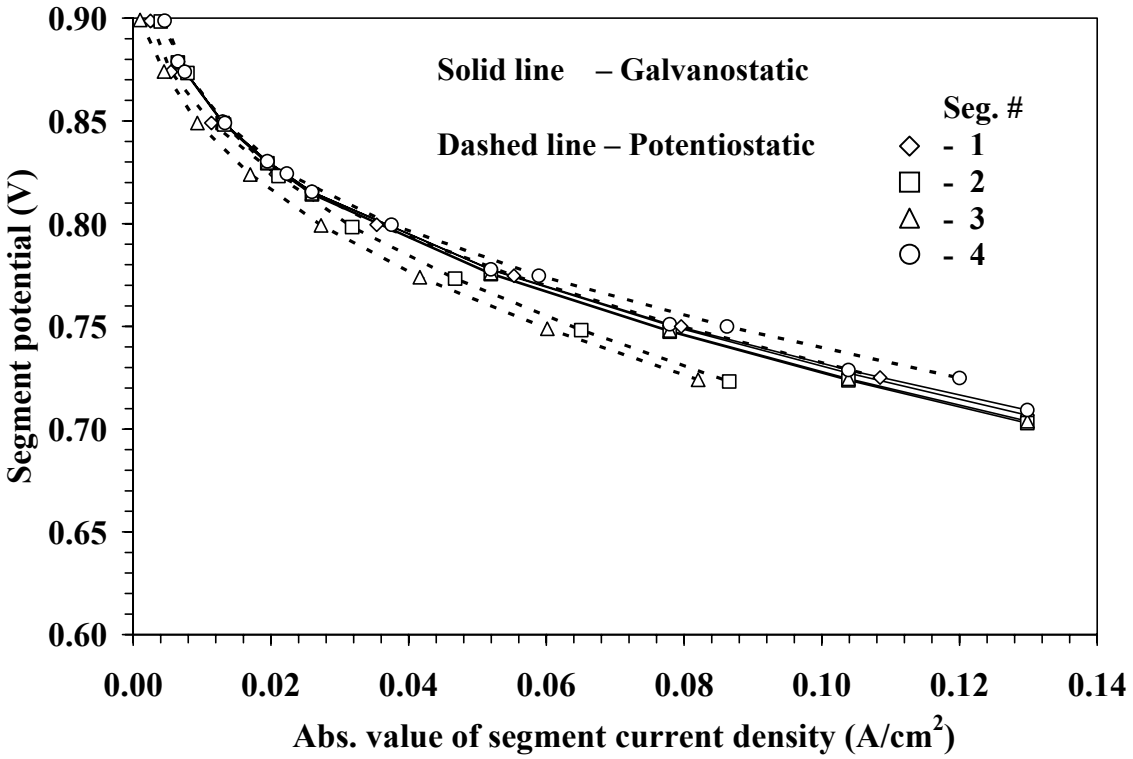

Figure 4. Galvanostatic and potentiostatic segment polarization curves using a common MEA with SIGRACET® GDL. H_2 flow rate = 2 A/cm^2, O_2 flow rate = 2 A/cm^2, H_2 humidifier temperature = 70°C, O_2 humidifier temperature = 25°C and Cell temperature = 30°C.

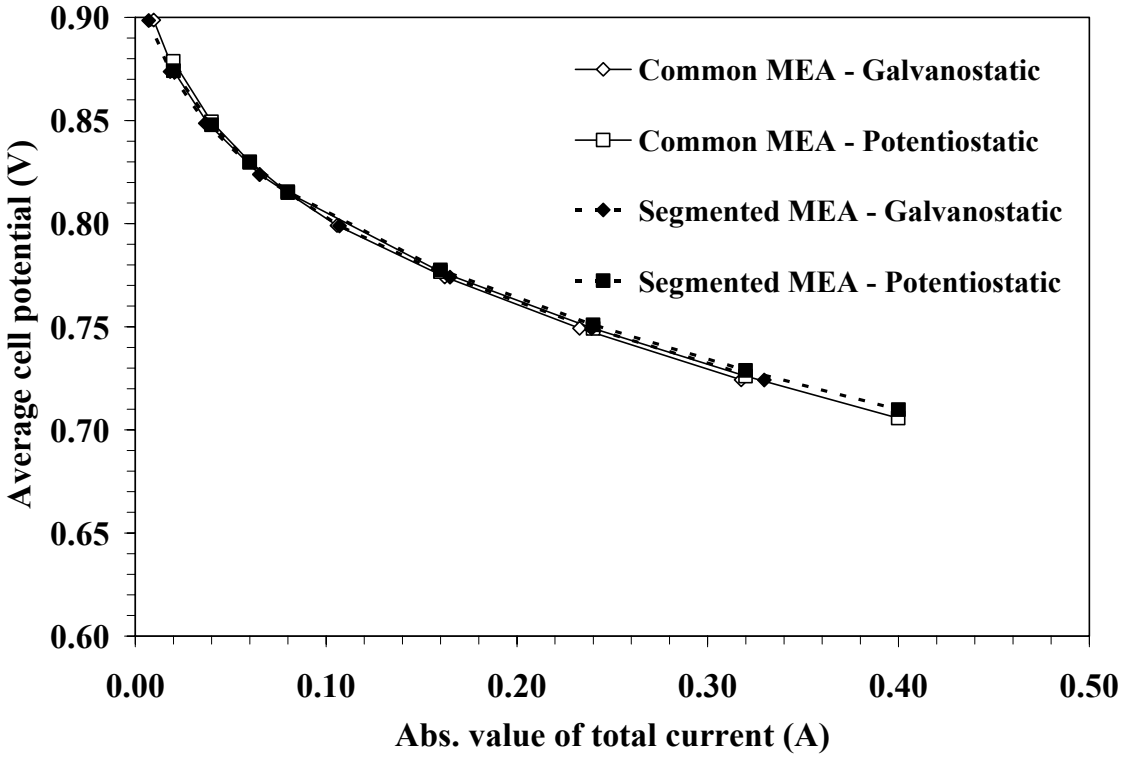

Figure 5. Comparison of total cell current of common and segmented MEAs under galvanostatic and potentiostatic discharge with SIGRACET® GDL. H_2 flow rate = 2 or 2.3 A/cm^2, O_2 flow rate = 2 or 2.3 A/cm^2, H_2 humidifier temperature = 70°C, O_2 humidifier temperature = 25°C and Cell temperature = 30°C.

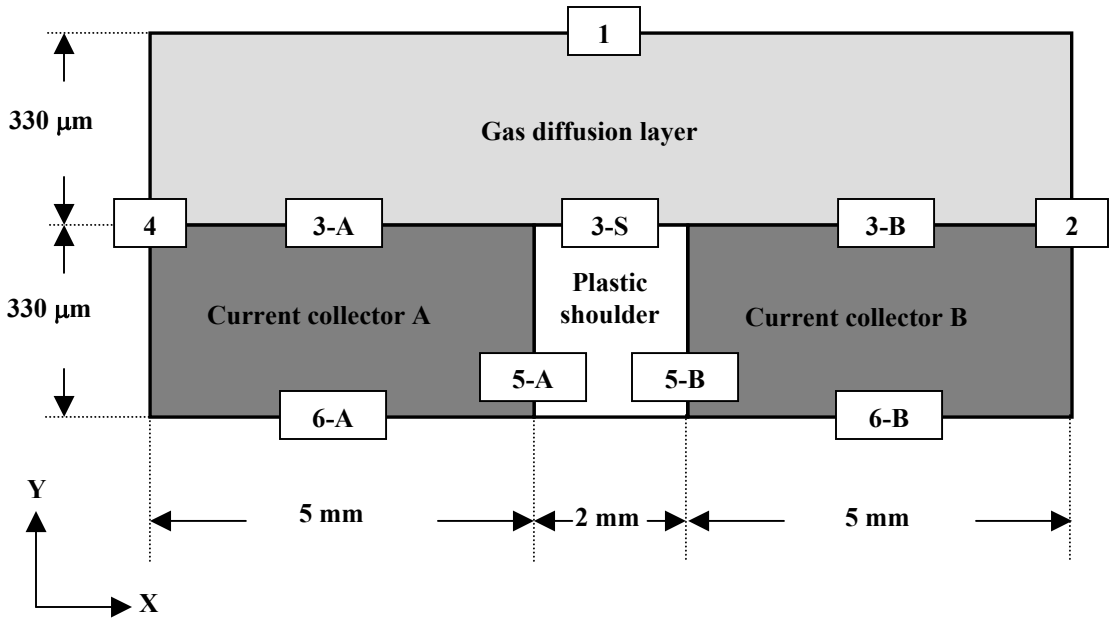

Figure 6: Schematic of the Model domain that includes the GDL, one half of two adjacent electrodes separated by plastic shoulder.

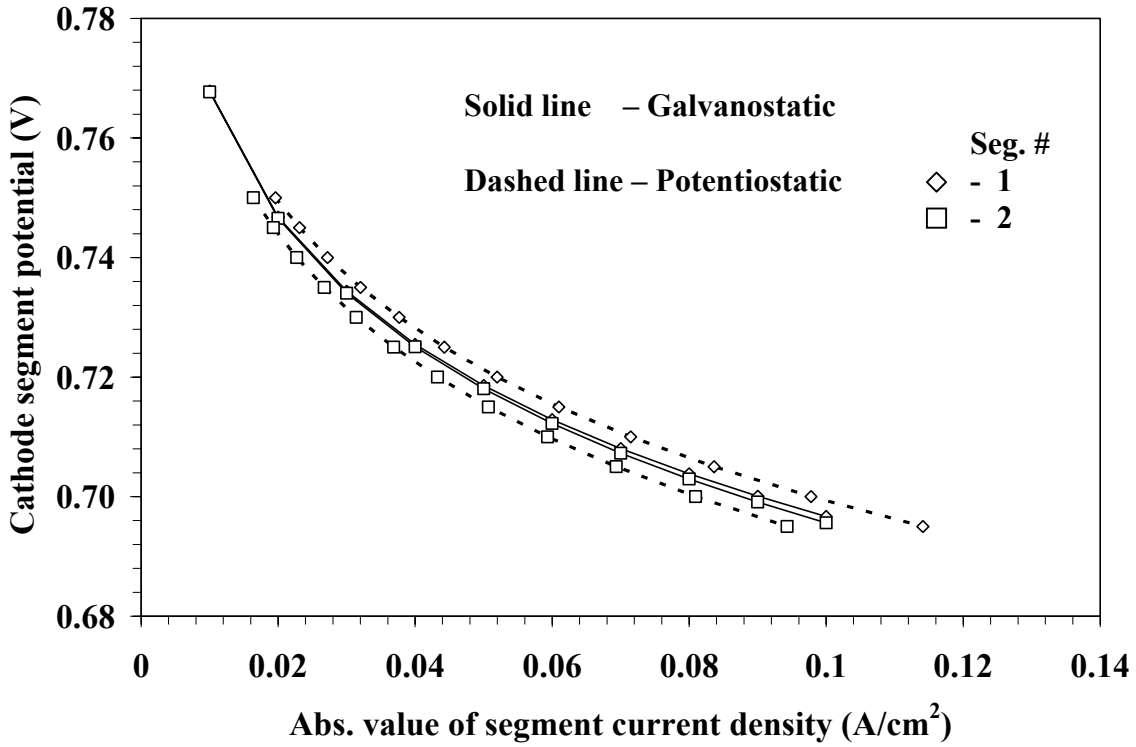

Figure 7: Galvanostatic and potentiostatic model simulations for a cathode made of common SIGRACET® GDL with non-uniform contact resistances (10.5 mΩ-cm^2 and 21 mΩ-cm^2 for current collectors A and B respectively)

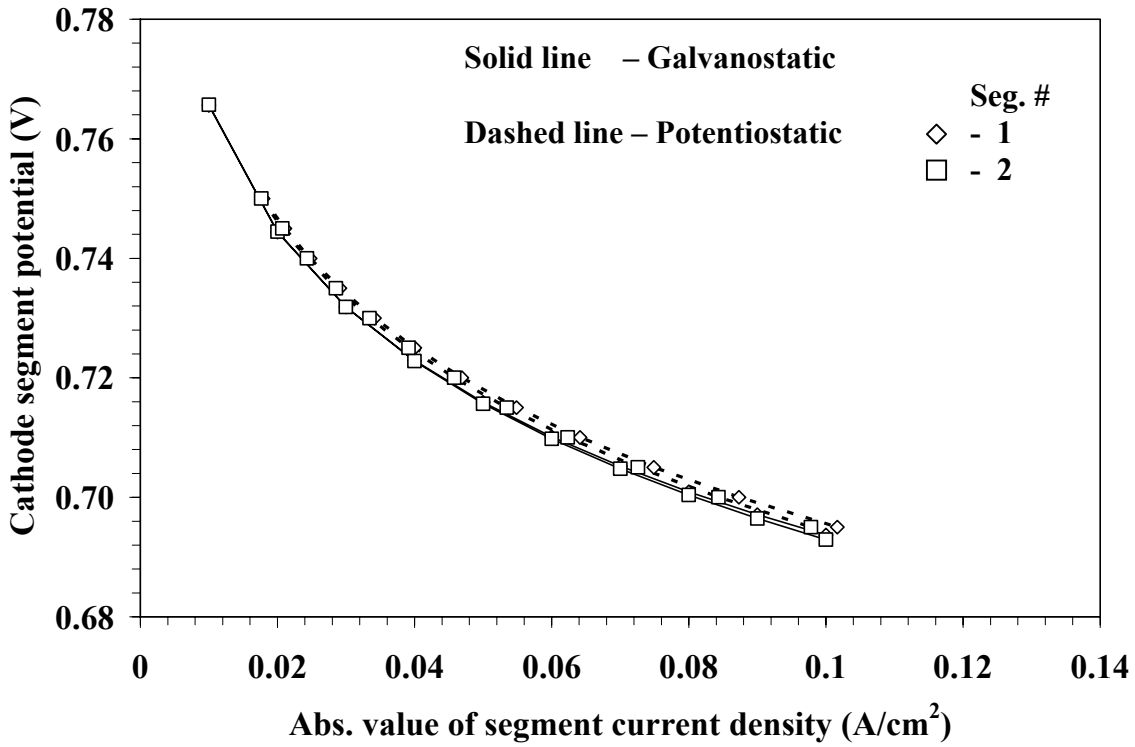

Figure 8: Galvanostatic and potentiostatic model simulations for a cathode with segmented SIGRACET® GDL.

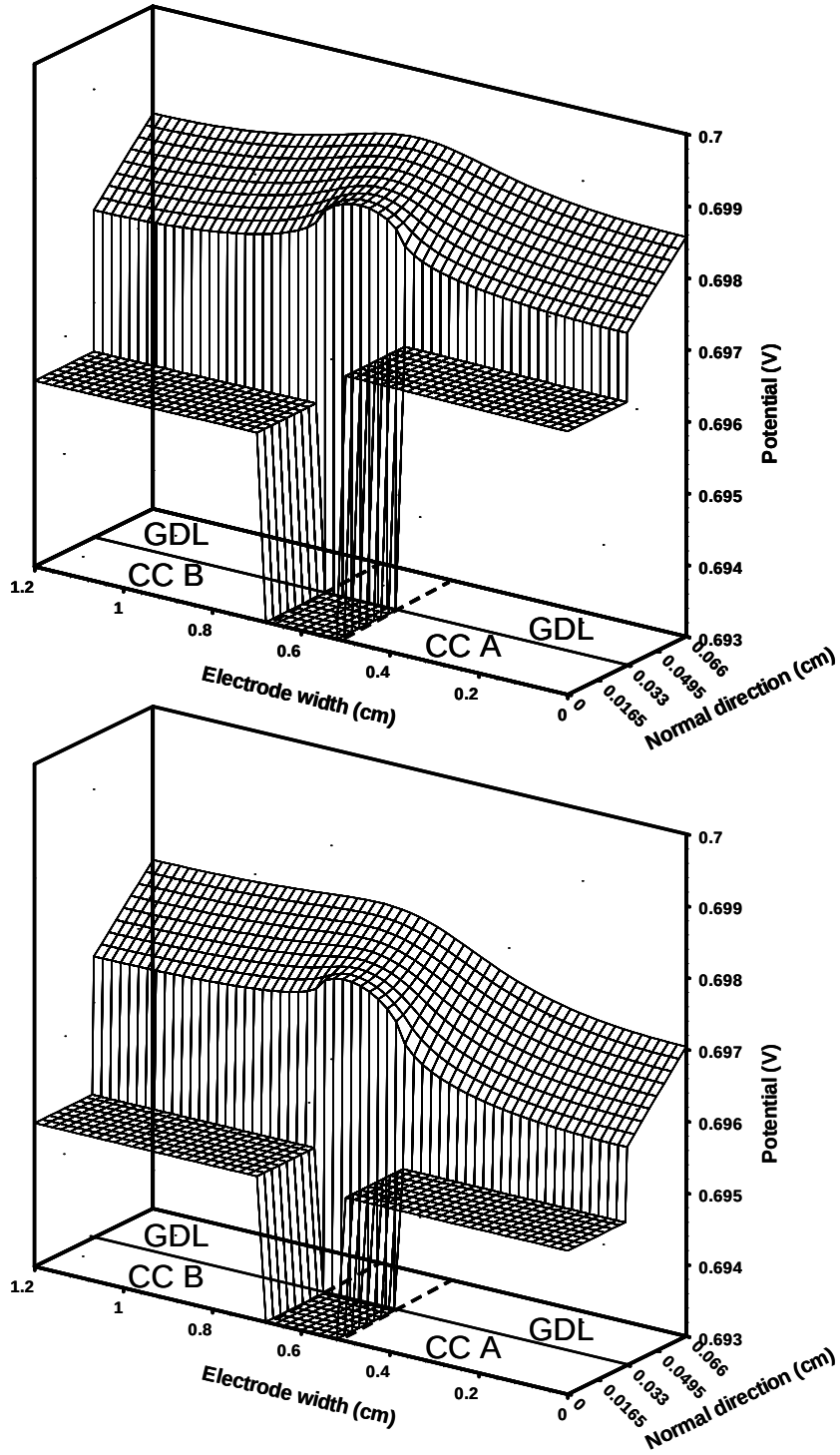

Figure 9: Model results of Potential distribution within the SIGRACET® GDL of the cathode for (a) Galvanostatic discharge and (b) Potentiostatic discharge

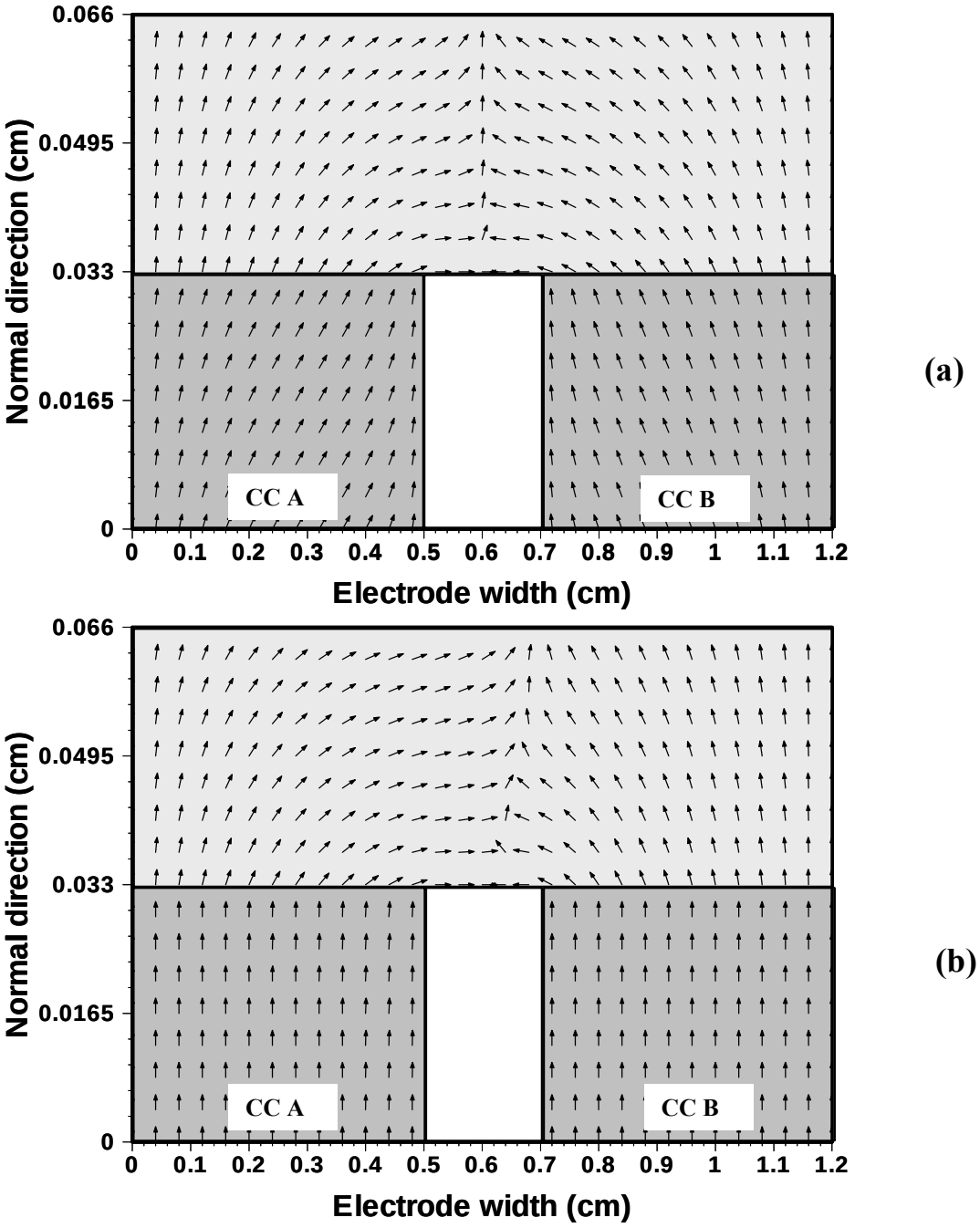

Figure 10: Model results of current vector distribution within the SIGRACET® GDL of the cathode for (a) Galvanostatic discharge and (b) Potentiostatic discharge (arrows sizes not scaled to the magnitude of the vector)

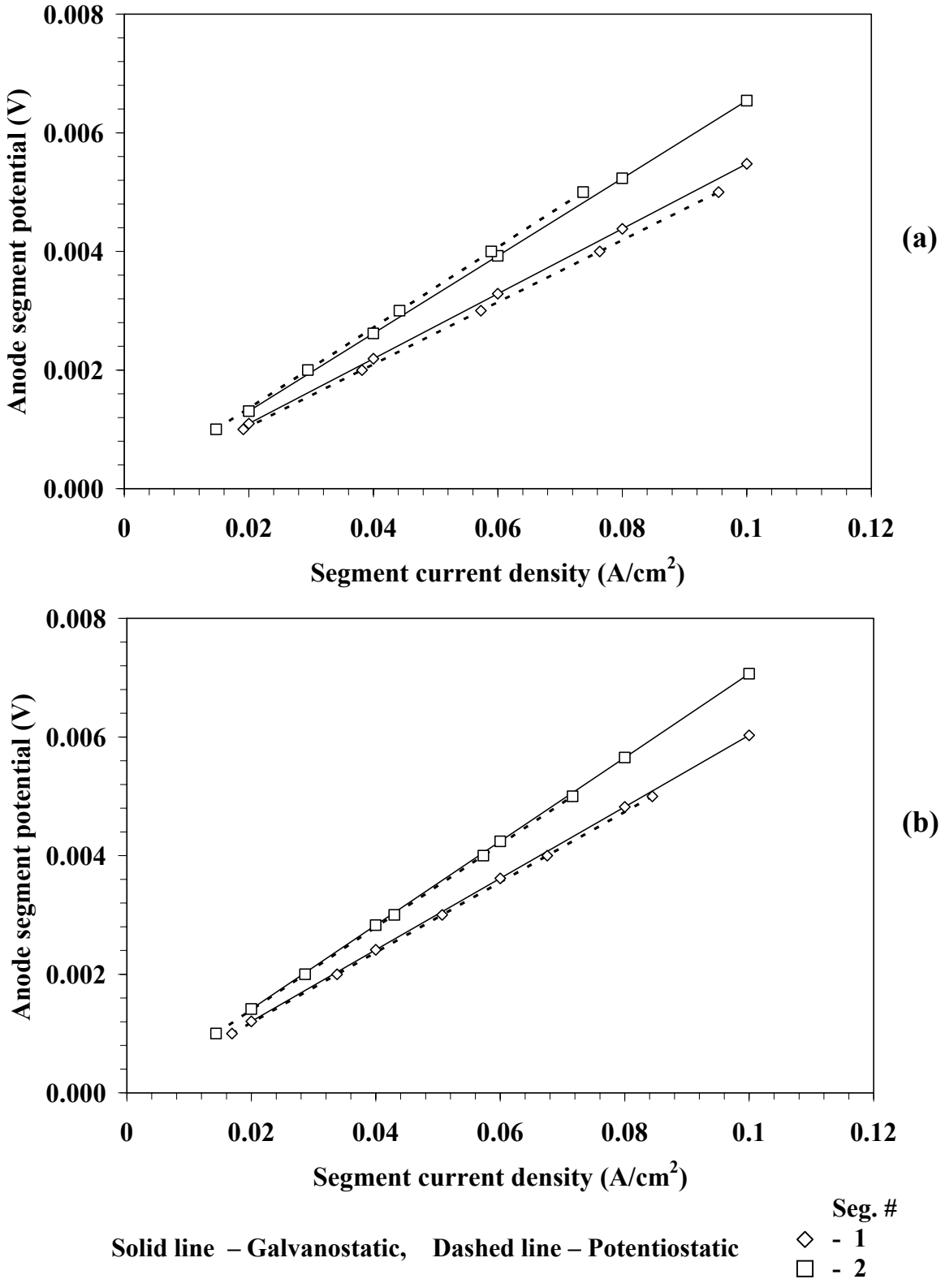

Figure 11: Galvanostatic and potentiostatic model simulations for an anode with (a) common SIGRACET® GDL (b) segmented SIGRACET® GDL.

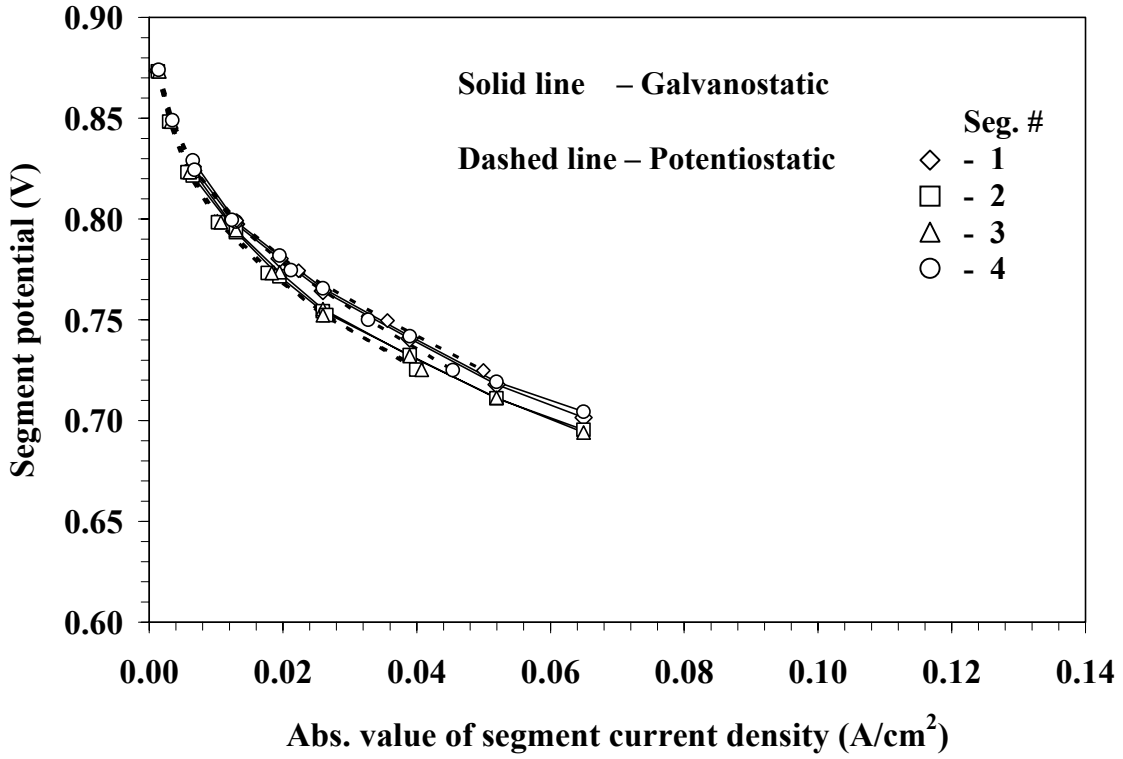

Figure 12. Galvanostatic and potentiostatic segment polarization curves using a segmented MEA with Toray® GDL. H_2 flow rate = 2.3 A/cm^2, O_2 flow rate = 2.3 A/cm^2, H_2 humidifier temperature = 70 °C, O_2 humidifier temperature = 25 °C and Cell temperature = 30 °C.

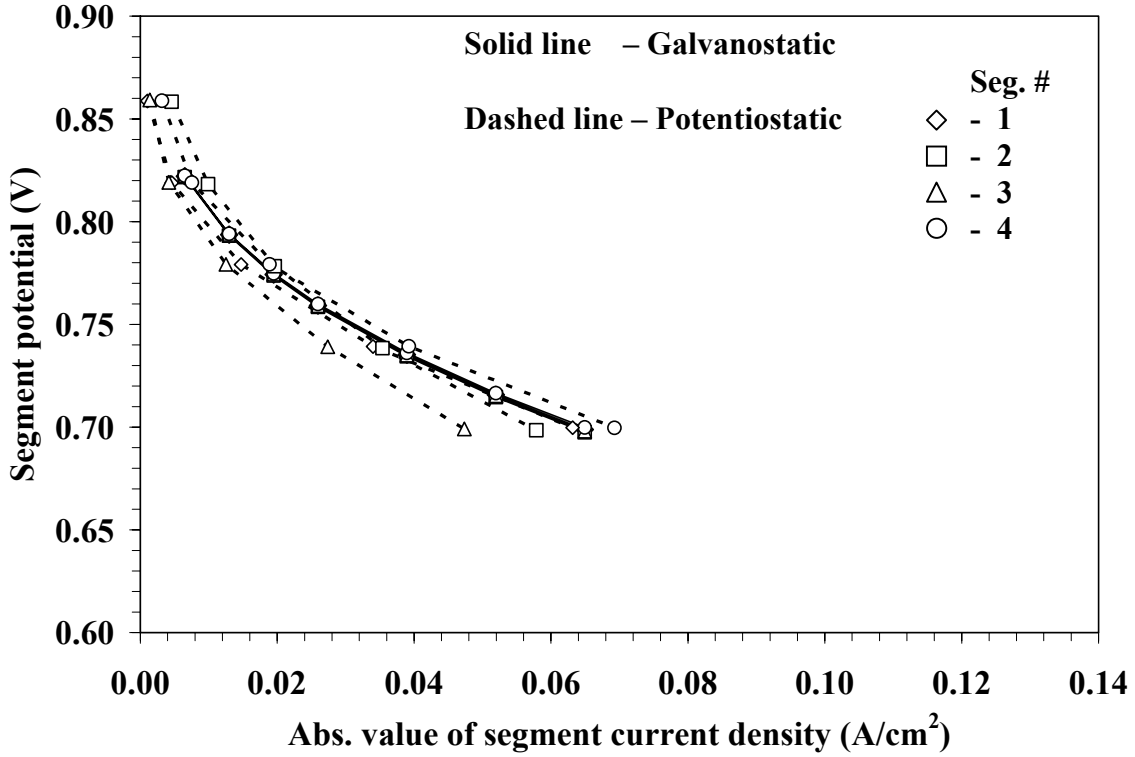

Figure 13. Galvanostatic and potentiostatic segment polarization curves using a common MEA with Toray® GDL. H_2 flow rate = 2 A/cm^2, O_2 flow rate = 2 A/cm^2, H_2 humidifier temperature = 70 °C, O_2 humidifier temperature = 25 °C and Cell temperature = 30 °C.

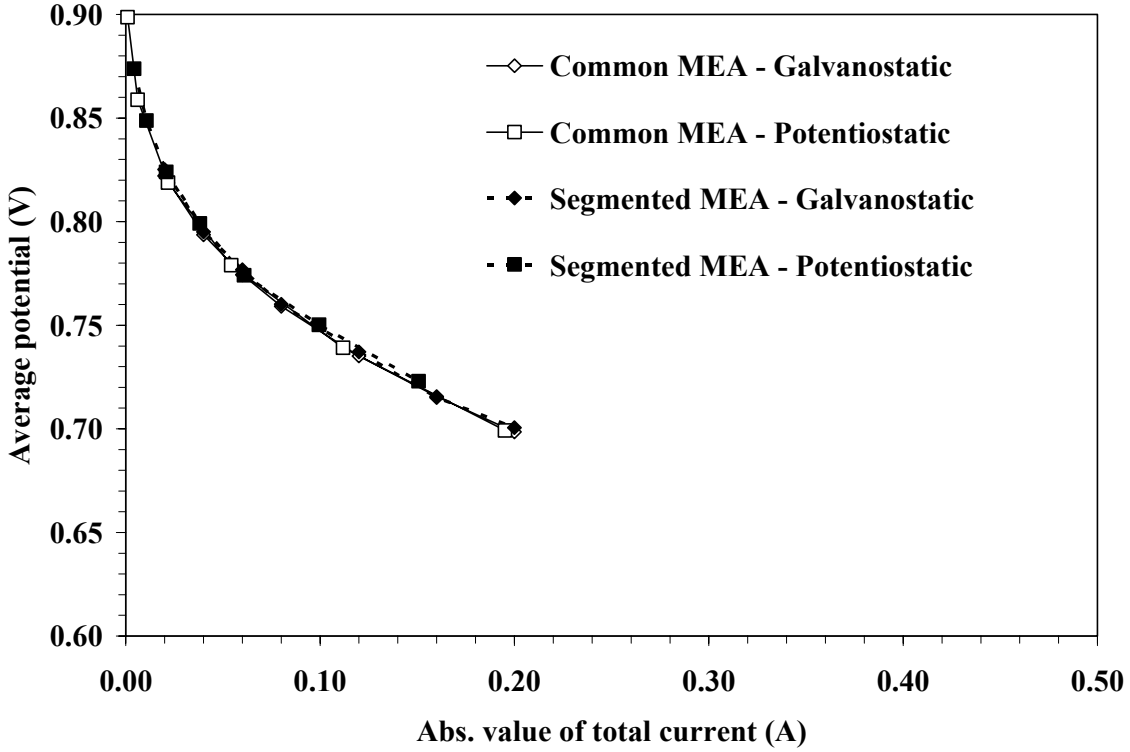

Figure 14. Comparison of total cell current of common and segmented MEAs under galvanostatic and potentiostatic discharge with Toray® GDL. H_2 flow rate = 2 or 2.3 A/cm^2, O_2 flow rate = 2 or 2.3 A/cm^2, H_2 humidifier temperature = 70 °C, O_2 humidifier temperature = 25 °C and Cell temperature = 30 °C.

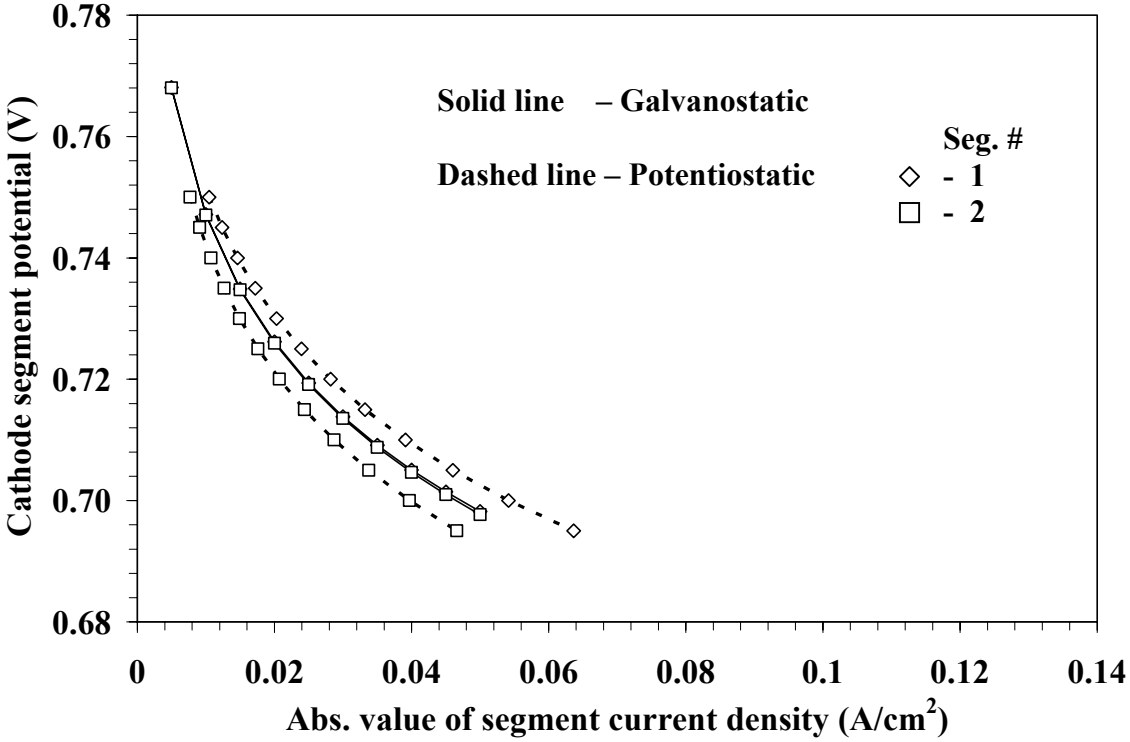

Figure 15: Galvanostatic and potentiostatic model simulations for the cathode with a common Toray® GDL .

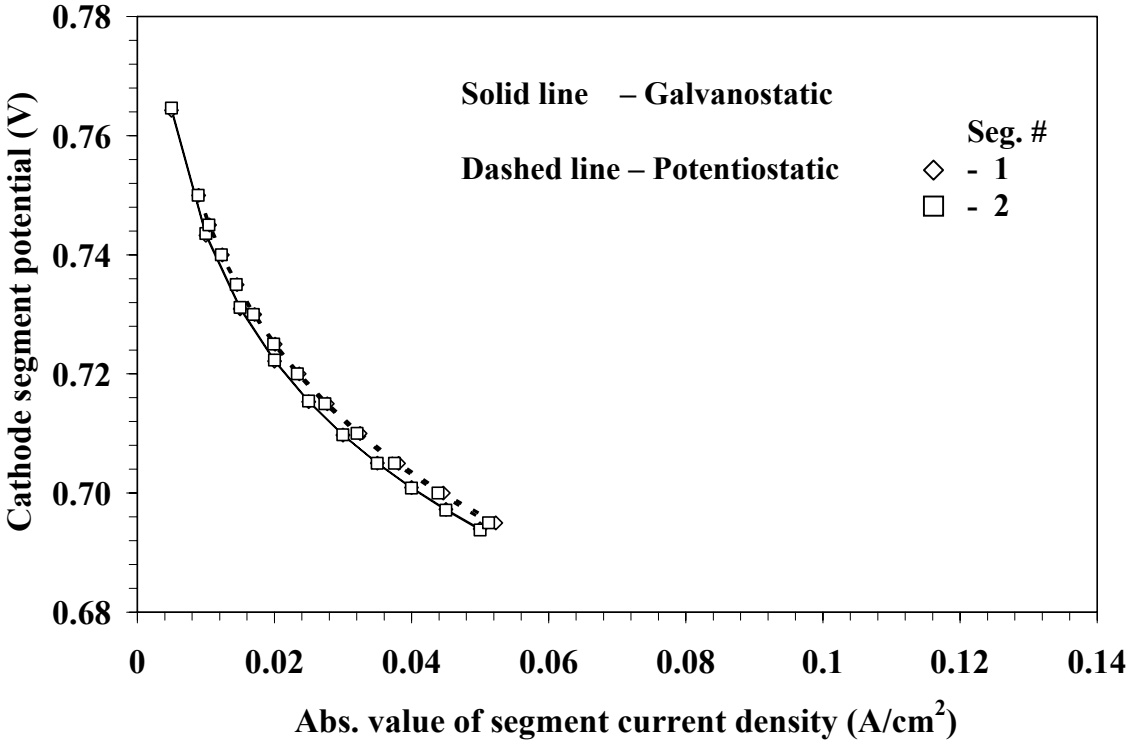

Figure 16: Galvanostatic and potentiostatic model simulations for the cathode with a segmented Toray® GDL .